This article has been accepted for publication in a future issue of this journal, but has not been fully edited. Content may change prior to final publication. Citation information: DOI 10.1109/TIP.2019.2948279, IEEE Transactions on Image Processing

Fast Single Image Dehazing Using Saturation Based Transmission Map Estimation

Se Eun Kim, Tae Hee Park, and Il Kyu Eom

***Abstract*—Single image dehazing has been a challenging problem because of its ill-posed nature. For this reason, numerous efforts have been made in the field of haze removal. This paper proposes a simple, fast, and powerful algorithm for haze removal. The medium transmission is derived as a function of the saturation of the scene radiance only, and the saturation of scene radiance is estimated using a simple stretching method. A different medium transmission can be estimated for each pixel because this method does not assume that transmission is constant in a small patch. Furthermore, this paper presents a color veil removing algorithm, which is useful for an image with fine or yellow dust, using the white balance technique. The proposed algorithm requires no training, prior, and refinement process. The simulation results show that the proposed dehazing scheme outperforms state-of-the-art dehazing approaches in terms of both computational complexity and dehazing efficiency.**

***Index Terms*—Single image dehazing, medium transmission, saturation stretch, white balance.**

I. Introduction

OUTDOOR images captured in inclement weather conditions have poor visibility caused by the absorption and scattering of light by atmospheric particles. Particles, such as dust and water droplets, reduce the light of an object along the line of sight. Because hazy images have poor contrast and color fidelity, they do not guarantee faithful results in vision applications. Therefore, haze removal, known as dehazing, is a challenging preprocessing method to improve the performance of various computer vision tasks.

Earlier dehazing approaches were based on multiple images or additional information because haze removal is an ill-posed problem. Polarization-based algorithms [1]-[3] have been used for image dehazing using multiple images of the same scene obtained with different degrees of polarization. Such methods can improve the visibility of hazy images and produce impressive results. On the other hand, it is difficult to find the maximum and minimum degrees of polarization under the same scene during rapid scene changes. Therefore, these methods are unsuitable for image restoration in real time. Multiple images of the same scene under different weather conditions were exploited to remove haze from images [4], [5]. These types of dehazing algorithms can achieve good results. Image dehazing is difficult to realize for real-time applications because two or more different images of the same scene are required.

In recent years, many studies have focused on using a single reference image for dehazing. Image enhancement-based haze removal methods have been initially proposed. These methods do not require image degradation models, but merely use various image processing techniques to improve the contrast and details of the image. These approaches include histogram-based [6], [7], Retinex-based [8]-[10], and transform domain enhancement algorithms [11]-[13]. Generally, image enhancement-based dehazing approaches cannot generate satisfactory results because they do not consider any image degradation model.

Popular dehazing methods are based on the physical image formation model in a scattering medium. These model-based approaches require reasonable assumptions and priors. Therefore, considerable efforts have been made to set up an appropriate prior for image dehazing. In 2008, Tan [14] introduced a contrast prior under the assumption that the local contrast of a haze-free image is significantly higher than that of a hazy image. Based on this assumption, he presented a dehazing algorithm by maximizing the local contrast of the image. This method easily causes color over-saturation in images with a heavy haze. To resolve the over-enhancing effects of Tan's algorithm, a range of variational frameworks [15]-[17] for dehazing have been presented.

Based on the prior knowledge that there is no correlation between object surface shading and transmission map, Fattal estimated the medium transmission map using the independent component analysis and Markov random field model [18]. This approach can produce impressive results when there is sufficient color information. On the other hand, this method cannot restore images with heavy haze and may fail in cases where the original assumptions are invalid.

He *et al*. [19] proposed a simple and effective dehazing method based on the dark channel prior (DCP). The basic concept of the DCP is that at least one color channel has extremely low intensity for most non-sky patches. In this approach, minimum filtering is used to produce a rough transmission map, and soft matting is adopted to refine the map

S. E. Kim is with the Department of Electronics Engineering, Pusan National University, 2, Busandaehak-ro 63 beon-gil, Geumjeong-gu, Busan, 46241, South Korea (e-mail: se-eun.kim@pusan.ac.kr).

T. H. Park is with 1Department of Mechatronics Engineering, Tong Myoung University, 428, Sinseon-ro, Nam-gu, Busan 48520 , South Korea (e-mail: thpark77@tu.ac.kr)

I. K. Eom is with the Department of Electronics Engineering, Pusan National University, 2, Busandaehak-ro 63 beon-gil, Geumjeong-gu, Busan, 46241, South Korea (e-mail: ikeom@pusan.ac.kr).

and obtain better performance. Owing to the effectiveness of the DCP, a majority of recent dehazing techniques have exploited this concept. Intensive efforts have been made to refine the coarse transmission map based on the DCP, such as bilateral filtering [20], [21], guided filtering [22], [23], median filtering [24], smooth filtering [25], and fusion-based approaches [26], [27]. Improving DCP is an issue for dehazing. A median DCP [28] was presented to improve He *et al*'s map by calculating the median neighborhood instead of the minimum value. Meng *et al*. [29] introduced a new geometric perspective for DCP using a boundary constraint. This method is fast and can attenuate the image noise and enhance interesting image structures. In addition to the aforementioned methods, many DCP-based dehazing approaches [30] have been proposed.

Most haze removal algorithms assume that the transmission and radiance are piece-wise constant, which leads to the use of a patch-based approach. For this reason, patch-based methods take significant care to avoid artifacts by the internal patch recurrence property [31], and multiple patches [32]. Berman *et al*. suggested a pixel-based dehazing algorithm using the haze-lines (HL) model [33] to improve their non-local image dehazing (NLD) method [34]. This model is based on the assumption that colors tend to repeat in natural scenes and are often located at different distances from the camera. This algorithm requires no training, and performs well on a wide variety of images. This method, however, shows failure cases when lighting is non-uniform and the sky shows unnatural colors. In addition, it incurs significant computational cost.

Recently, machine learning-based dehazing approaches have become popular. Cai *et al*. provided DehazeNet [35], which is a deep learning model for single image dehazing. By accepting a hazy image as input, DehazeNet calculates and outputs its corresponding transmission map. The limitation of this method is that fixed global atmospheric light is less accurate than dynamic local light. A multiscale convolutional neural network (MSCNN) based dehazing approach was presented [36]. This algorithm first generates a coarse-scale transmission matrix and then refines it gradually. An all-in-one dehazing network (AOD-Net) [37] was used to generate a haze-free image directly via a CNN and exploited a local airlight estimation for better results. Zhang *et al*. proposed a densely connected pyramid dehazing network (DCPDN) [38] to learn the transmission map, and atmospheric light jointly. This method exploited an encoder-decoder architecture with a multilevel pyramid pooling module to learn multi-scale features. Ren *et al*. presented a gated fusion network (GFN) [39] by adopting an encoder-decoder architecture. GFN adopted a fusion-based strategy that derives three inputs from an original hazy image by applying white balance, contrast enhancing, and Gamma correction. A fully point-wise CNN (FPCNN) [40] for modeling statistical regularities in natural images was proposed to remove haze. This method shuffled the pixels randomly in the original image and leveraged the shuffled image as input to make CNN more concerned with the statistical properties. Xu *et al*. proposed an encoder-decoder architecture as an end-to-end system for single image dehazing [41]. This network has an encoder-decoder architecture with skip connections and instance normalization, and adopts the convolutional layers of a pre-trained VGG network as an encoder to exploit the representation power of deep features. Yang *et al*. provided a disentangled dehazing network (DDN) [42], which is an end-to-end model that generates realistic haze-free images using only unpaired supervision. This approach alleviated the paired training constraint by introducing a physical model-based disentanglement and reconstruction mechanism. Yang *et al*. proposed a proximal dehaze network (PDN) [43], which is a deep learning approach for single image dehazing by learning the dark channel and transmission priors. This network combines the advantages of traditional prior-based dehazing methods and deep learning methods by incorporating haze-related prior learning into a deep network. Haze removal methods based on deep learning show promising results, but, the results can be affected by the training dataset.

Generally, haze increases the brightness of an image and reduces saturation. Haze removal studies considering image saturation have been reported. In [44], a color attenuation prior (CAP), which assumed that the brightness and saturation of pixels in a hazy image vary sharply along with the change in the haze concentration, was used for image dehazing. Under this prior, a linear model for modeling the scene depth of hazy images was developed, and the parameters of this model were obtained by supervised learning. A transmission estimation method for image dehazing using saturation and intensity was reported [45]. In this method, the authors assumed that all atmospheric lights are the same, and local patches share the same transmission map. The initial transmission map was calculated based on these assumptions. This algorithm requires refinement and post-processing to estimate the transmission more precisely.

In this paper, we propose a new and fast estimation method of medium transmission based on the saturation of an image for single image dehazing. The medium transmission is derived on a pixel-by-pixel basis without any prior. The transmission of this method is a function only of the saturation under the assumption that the atmospheric light is known. Furthermore, we present an efficient method based on white balancing to remove the color veil in the image generated in yellow or fine dust. The proposed method is fast, requires no training and refinement, and generates reasonable dehazing results on a wide variety of images.

The remainder of this paper is organized as follows. Section II introduces the atmospheric scattering model for dehazing. Section III presents details of the proposed method. Section IV reports and discusses the experimental results. Finally, the concluding remarks are given in Section V.

II. Atmospheric Scattering Model

A hazy image can be modeled as a convex sum of a haze-free image and the atmospheric light traveling through air. The formation of a hazy image is usually described by the atmospheric scattering model [46] as follows.

This article has been accepted for publication in a future issue of this journal, but has not been fully edited. Content may change prior to final publication. Citation information: DOI 10.1109/TIP.2019.2948279, IEEE Transactions on Image Processing

$$E(d,\lambda) = e^{-\beta(\lambda)d} E_0(\lambda) + \left[1 - e^{-\beta(\lambda)d}\right] E_\infty(\lambda), \quad (1)$$

where λ is the wavelength of visible light, d is the distance from the scene to the camera, and $\beta(\lambda)$ is the atmospheric scattering coefficient. The first term on the right-hand side of (1) is the direct attenuation, which describes the attenuation result of light reflected in the medium, and the second term is the airlight, which represents scattering of global atmospheric light. By letting $\mathbf{H}(\mathrm{x})=E(d,\lambda)$, $\mathbf{J}(\mathrm{x})=E_0(\lambda)$, $t(\mathrm{x})=e^{-\beta(\lambda)d}$, and $\mathbf{A}=E_\infty(\lambda)$, (1) can be simplified to

$$\mathbf{H}(\mathrm{x}) = t(\mathrm{x})\mathbf{J}(\mathrm{x}) + \left[1 - t(\mathrm{x})\right]\mathbf{A}, \quad (2)$$

where $\mathrm{x}=(x,y)$ is the position of the pixel within the image, $\mathbf{H}(\mathrm{x})$ is the hazy image, $\mathbf{J}(\mathrm{x})$ is the scene radiance representing the haze-free image, $\mathbf{A}$ is the atmospheric light, and $t(\mathrm{x})$ is the medium transmission describing the portion of light that is not scattered. In general, $\beta(\lambda)$ is wavelength dependent. Therefore $t(\mathrm{x})$ is different per color channel. In almost all haze removal approaches, this dependency has been assumed to be negligible to reduce the number of unknowns. The boldface symbols ($\mathbf{H}$, $\mathbf{J}$, and $\mathbf{A}$) represent the vectors that have three color components.

The goal of dehazing is to recover $\mathbf{J}(\mathrm{x})$ from $\mathbf{H}(\mathrm{x})$. This is an ill-posed problem because there are unknown $\mathbf{J}(\mathrm{x})$, $t(\mathrm{x})$, and $\mathbf{A}$ items in a single equation. $\mathbf{J}(\mathrm{x})$ can be estimated from a single image if some prior knowledge is available, or if the depth information of an image is known. From the estimated transmission map and atmospheric light, the scene radiance can be restored by

$$\mathbf{J}(\mathrm{x}) = D\left(\mathbf{H}(\mathrm{x}), \mathbf{A}, t(\mathrm{x})\right) = \frac{\mathbf{H}(\mathrm{x}) - \mathbf{A}}{t(\mathrm{x})} + \mathbf{A}, \quad (3)$$

where $D(\cdot)$is the dehazing function when the hazy image, atmospheric light, and transmission map are given.

III. Proposed Method

A. Basic Formulation for Transmission Map

When atmospheric light $\mathbf{A}$ is assumed to be given, the haze imaging equation in (2) can be normalized by $\mathbf{A}$ as follows.

$$\frac{H^c(\mathrm{x})}{A^c} = t(\mathrm{x})\frac{J^c(\mathrm{x})}{A^c} + 1 - t(\mathrm{x}),\ c \in \{r,g,b\}, \quad (4)$$

where $H^c(\mathrm{x})$, $J^c(\mathrm{x})$, and A^c are color channels of $\mathbf{H}(\mathrm{x})$, $\mathbf{J}(\mathrm{x})$, and $\mathbf{A}$, respectively. In the DCP-based dehazing approaches, transmission in a local patch $\Omega(\mathrm{x})$ is assumed to be constant. The dark channel on both sides of Eq. (4) is as follows.

$$\min_{\mathrm{y}\in\Omega(\mathrm{x})}\left(\min_c \frac{H^c(\mathrm{y})}{A^c}\right) = t(\mathrm{x}) \min_{\mathrm{y}\in\Omega(\mathrm{x})}\left(\min_c \frac{J^c(\mathrm{y})}{A^c}\right) + 1 - t(\mathrm{x}). \quad (5)$$

The dark channel of $\mathbf{J}$ is close to zero owing to the dark channel prior, that is,

$$J^{\mathrm{dark}}(\mathrm{x}) = \min_{\mathrm{y}\in\Omega(\mathrm{x})}\left(\min_c J^c(\mathrm{y})\right) \approx 0. \quad (6)$$

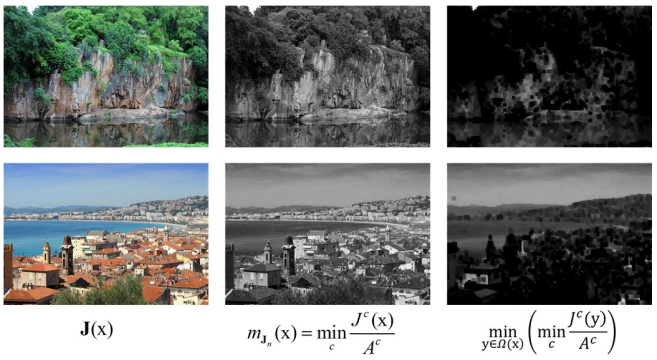

Fig. 1. Examples of $m_{\mathbf{J}_n}(\mathrm{x})$ and dark images. Left: natural image, middle: minimum image by (7), right: dark image by dark channel prior.

Many haze reduction methods have been presented based on two assumptions (dark channel prior and constant transmission in a local patch). These two assumptions lead to a simple and useful dehazing framework. However, $J^{\mathrm{dark}}(\mathrm{x})$ is not always zero, and transmission is not constant in a local patch. These facts produce annoying artifacts in the dehazed image. Therefore, a range of post-processing methods such as soft matting [19], bilateral filtering [20], [21] and guided filtering [22], [23] are followed by a transmission estimation.

In this paper, we assume that transmission differs from pixel to pixel. The following equation is obtained using the minimum operation on (4),

$$\min_c H_n^c = t(\mathrm{x}) \min_c J_n^c + 1 - t(\mathrm{x}), \quad (7)$$

where $H_n^c(\mathrm{x}) = {}^{H^c(\mathrm{x})}\!/_{A^c}$, and $J_n^c(\mathrm{x}) = {}^{J^c(\mathrm{x})}\!/_{A^c}$. This equation can be rearranged to

$$t(\mathrm{x}) = \frac{1 - m_{\mathbf{H}_n}(\mathrm{x})}{1 - m_{\mathbf{J}_n}(\mathrm{x})}, \quad (8)$$

where $m_{\mathbf{H}_n}(\mathrm{x}) = \min_c H_n^c(\mathrm{x})$, and $m_{\mathbf{J}_n}(\mathrm{x}) = \min_c J_n^c(\mathrm{x})$. Fig. 1 shows some examples of $m_{\mathbf{J}_n}(\mathrm{x})$ of natural haze-free images. The dark images generated by (6) are also shown in Fig. 1. As shown in Fig. 1, the dark channel prior is not working under the condition that the transmission is not constant in a local patch. The images formed by $m_{\mathbf{J}_n}(\mathrm{x})$ look like gray images. From Fig. 1, $m_{\mathbf{J}_n}(\mathrm{x})$ is not always zero. Moreover, the dark images obtained by the DCP are not zero in the bright background regions. Therefore, the dark channel prior is a limited assumption that cannot be used extensively in all image areas. In this paper, we present a new dehazing framework for estimating a pixel-wise transmission map without the DCP.

This article has been accepted for publication in a future issue of this journal, but has not been fully edited. Content may change prior to final publication. Citation information: DOI 10.1109/TIP.2019.2948279, IEEE Transactions on Image Processing

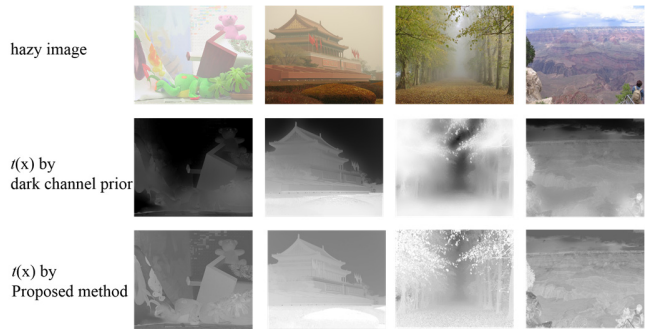

Fig. 2. Transmission maps obtained by the dark channel prior and proposed method.

B. Transmission Map Estimation

This section presents a saturation-based transmission map estimation method. Let $S_{\mathbf{K}}(x)$ be the saturation component at location x for a given image, $\mathbf{K}(x)$, which is defined as

$$S_{\mathbf{K}}(x) = 1 - \frac{m_{\mathbf{K}}(x)}{I_{\mathbf{K}}(x)}, \tag{9}$$

where $m_{\mathbf{K}}(x) = \min_{c\in\{r,g,b\}} K^c(x)$, and $I_{\mathbf{K}}(x)$ is the intensity of $\mathbf{K}(x)$, that is,

$$I_{\mathbf{K}}(x) = \frac{K^r(x) + K^g(x) + K^b(x)}{3}. \tag{10}$$

Using $m_{\mathbf{K}}(x)=I_{\mathbf{K}}(x)(1-S_{\mathbf{K}}(x))$ from (9), Eq. (8) can be rewritten as

$$t(x) = \frac{1 - I_{\mathbf{H}_n}(x)\left(1 - S_{\mathbf{H}_n}(x)\right)}{1 - I_{\mathbf{J}_n}(x)\left(1 - S_{\mathbf{J}_n}(x)\right)}. \tag{11}$$

Thus far, the transmission map can be determined by the intensity and saturation of the normalized scene radiance. Two unknowns ($I_{\mathbf{J}_n}(x)$ and $S_{\mathbf{J}_n}(x)$) are used to estimate $t(x)$.

By normalizing (3) to $\mathbf{A}$, $I_{\mathbf{J}_n}(x)$ was estimated using (4) and (10) as follows.

$$I_{\mathbf{J}_n}(x) = \frac{I_{\mathbf{H}_n}(x) - 1}{t(x)} + 1. \tag{12}$$

By combining (11) and (12), $t(x)$ is obtained as

$$t(x) = \frac{1 - I_{\mathbf{H}_n}(x)\left(1 - S_{\mathbf{H}_n}(x)\right)}{1 - \left(\frac{I_{\mathbf{H}_n}(x) - 1}{t(x)} + 1\right)\left(1 - S_{\mathbf{J}_n}(x)\right)}. \tag{13}$$

This is a first-order equation for $t(x)$. Therefore, $t(x)$ can be obtained analytically as follows.

$$t(x) = 1 - I_{\mathbf{H}_n}(x)\left(1 - \frac{S_{\mathbf{H}_n}(x)}{S_{\mathbf{J}_n}(x)}\right). \tag{14}$$

As shown in (14), the transmission map at location x is estimated in a simple form using single unknown value $S_{\mathbf{J}_n}(x)$. If $S_{\mathbf{J}_n}(x)$ is estimated, $t(x)$ can be obtained. Estimating $S_{\mathbf{J}_n}(x)$ is much easier than estimating $m_{\mathbf{J}_n}(x)$ directly. The estimation method for $S_{\mathbf{J}_n}(x)$ will be discussed in the next section. Fig. 2 shows examples of the dark channel prior based transmission map after guided filtering and the proposed transmission map. The transmission maps obtained by the dark channel prior cannot represent the detailed textures and edges of the image, because they are produced by a local patch.

When the local patch $\Omega(x)$ is a 1x1 window, the proposed transmission map is a general equation that can include the dark channel prior-based dehazing equation. If $m_{\mathbf{J}_n}(x) \to 0$, then $S_{\mathbf{J}_n}(x) \to 1$. This condition leads $t(x)$ to $t(x) \to 1 - m_{\mathbf{H}_n}(x)$, which is, $t(x) \to 1 - \min_c {}^{H^c}\!/_{A^c}$. This is the DCP-based transmission map when $\Omega(x)$ is assumed to be a 1x1 window.

A transmission estimation method for image dehazing using saturation and intensity was reported in 2018 [45]. They assumed that all atmospheric lights are the same, and local patches share the same transmission map. From these assumptions, the transmission map is calculated in the following form.

$$\hat{t}(x) = 1 - \psi \frac{I_{\mathbf{H}}(x)}{A}\left(1 - \frac{S_{\mathbf{H}}(x)}{S_{\mathbf{J}}(x)}\right), \tag{15}$$

where ψ is the fitting coefficient used to adjust the degree of refinement of the initial transmission map. The initial transmission $\hat{t}(x)$ was smoothed into a refined transmission by minimizing the defined cost function. In addition, this method assumed that all atmospheric lights are the same. In this paper, we remove all assumptions through the process of normalizing the color component to the corresponding atmospheric light. For this reason, no refinement and post-processing methods are needed to estimate the transmission map in the proposed algorithm.

C. Estimating Saturation of Scene Radiance

The aim in this section is to estimate $S_{\mathbf{J}_n}(x)$. The first step is to find the constraint of $S_{\mathbf{J}_n}(x)$. From (14),

$$S_{\mathbf{H}_n}(x) = t(x)\frac{I_{\mathbf{J}_n}(x)}{I_{\mathbf{H}_n}(x)} S_{\mathbf{J}_n}(x). \tag{16}$$

This article has been accepted for publication in a future issue of this journal, but has not been fully edited. Content may change prior to final publication. Citation information: DOI 10.1109/TIP.2019.2948279, IEEE Transactions on Image Processing

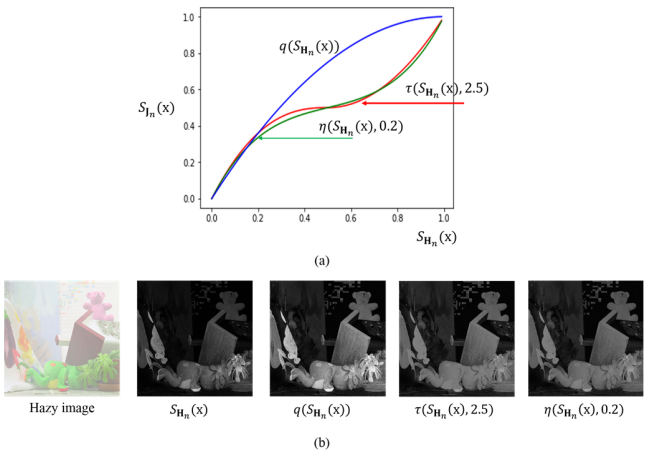

Fig. 3. Example of saturation stretching function. (a) graphs of the three stretching functions, and (b) stretched saturations for a sample hazy image are represented in gray image form.

The relationship between $I_{\mathbf{H}_n}(x)$ and $I_{\mathbf{J}_n}(x)$ from (12) can also be obtained as follows.

$$I_{\mathbf{H}_n}(x) = t(x) I_{\mathbf{J}_n}(x) + 1 - t(x) . \tag{17}$$

From (16) and (17), $I_{\mathbf{J}_n}(x) \le I_{\mathbf{H}_n}(x)$ and $S_{\mathbf{J}_n}(x) \ge S_{\mathbf{H}_n}(x)$ can be derived easily because $0 \le t(x) \le 1$. Here, an approximate condition of $S_{\mathbf{J}_n}(x) \ge S_{\mathbf{H}_n}(x)$ is obtained. In this paper, we will show experimentally that this rough condition is sufficient for haze removal.

The contrast stretch concept is adopted to estimate $S_{\mathbf{J}_n}(x)$. The common contrast stretch algorithm produced successful results in many image processing applications. Three examples of the simple stretch function that satisfies the condition $S_{\mathbf{J}_n}(x) \ge S_{\mathbf{H}_n}(x)$ are discussed. The first stretch function is

$$\tau(z, p) = \begin{cases} 0.5\left(1 - \left(1 - \dfrac{z}{0.5}\right)^p\right), & z \le 0.5 \\ 0.5 + 0.5\left(\dfrac{z - 0.5}{0.5}\right)^2, & 0.5 < z \le 1 \end{cases} , \tag{18}$$

where $\tau(z, p)$ is the adaptive stretch function for z, $p (p>0)$ is the power constant. The second is defined as

$$q(z) = z(2 - z) . \tag{19}$$

In (19), $q(z)$ is the quadratic function of z with maximum value 1 at $z=1$. Finally, the third saturation function is used as follows.

$$\eta(z, \gamma) = \frac{\left(z^{\frac{1}{\gamma}} + \left(1 - (1 - z)^{\frac{1}{\gamma}}\right)\right)}{2} , \tag{20}$$

Fig. 4. Dehazed images using various stretch functions. (a) hazy image, (b) dehazed image using $\tau(z, p=2.5)$, (c) dehazed image using $q(z)$, and (d) dehazed image using $\eta(z, \gamma=0.2)$.

where $\eta(z, \gamma)$ is the stretch function defined in (20), and γ is the constant that determines the shape of $\eta(z, \gamma)$. The saturation of the normalized scene radiance can be estimated using (18), (19) or (20).

Fig. 3 shows example of the three stretch functions. Fig. 3(a) presents graphs of these stretch functions. In Fig. 3(b), the stretched saturations for a sample hazy image are represented in gray image form. Other choices may be possible to estimate $S_{\mathbf{J}_n}(x)$. Fig. 4 shows dehazed images using various stretch functions. As shown in Fig. 4, the dehazing performance does not depend largely on the stretch function.

D. Removing Color Veil

The hazy image is considered to be a convex sum of the haze-free image and veil made by atmospheric light. In general, it is assumed that all atmospheric light is similar because the haze has little color component. However, color veils may be present in yellow dust or certain lighting conditions. Fig. 5 gives examples of a hazy image with a color veil and its dehazed version. The top line in Fig. 5 shows a gray veil because all atmospheric light is similar, and the dehazed image has good visual quality. The middle line represents a color veil with larger red and blue values compared to that of the green component. The bottom line presents an ocher color veil, which can be seen as a typical veil when there is yellow dust. As shown in Fig. 5, the recovered images with a color veil do not show good dehazing performance (middle and bottom lines).

In this paper, we present a simple color veil removing algorithm using the white balancing method. The white balanced image for $\mathbf{H}(x)$, $\mathbf{H}_{WB}(x)$ is obtained as follows.

$$H^c_{WB}(x) = W\left(H^c(x)\right) = \frac{\mu\left(H^g(x)\right)}{\mu\left(H^c(x)\right)} H^c(x) , \tag{21}$$

where $\mu(H^c(x))$ is the average of color component $H^c(x)$, and $W(\cdot)$ is the white balancing function. $\mathbf{A}_{WB}$, which is the atmospheric light of the whited balanced hazy image, is obtained from $\mathbf{H}_{WB}(x)$. A larger deviation of the atmospheric

This article has been accepted for publication in a future issue of this journal, but has not been fully edited. Content may change prior to final publication. Citation information: DOI 10.1109/TIP.2019.2948279, IEEE Transactions on Image Processing

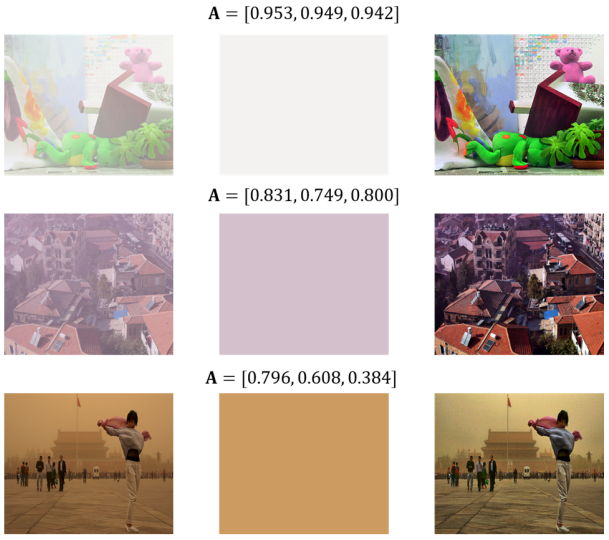

Fig. 5. Example of a hazy image with color veil and its dehazed version. (a) hazy image, (b) veil image constructed by atmospheric light, and (c) dehazed image.

light values means the haze veil has a large color component. Therefore, the deviations of **A** and $\mathbf{A}_{WB}$, are compared to determine whether to apply the white balance to remove haze.

Let $\Delta(\mathbf{y})$ be the difference between the maximum and minimum values of **y**. If $\Delta(\mathbf{A}) \le \Delta(\mathbf{A}_{WB})$, then the white b alancing process increases the difference between the maximum and minimum values of **A**. Therefore, it is assumed that the atmospheric veil of **H**(x) has little chromatic component. In this case, the dehazed image $\mathbf{J}(x)=D(\mathbf{H}(x),\mathbf{A},t(x))$ is obtained using (3). On the other hand, if $\Delta(\mathbf{A})>\Delta(\mathbf{A}_{WB})$, the white balancing process weakens the chromatic component of the atmospheric veil because of the gray-world assumption. Therefore, haze removal can be performed by $\mathbf{J}(x)=W[D(\mathbf{H}(x),\mathbf{A}_{WB},t(x))]$. Overall, we present an effective and automated dehazing algorithm that can respond selectively to color veils. For a given hazy image **H**(x), the dehazed image **J**(x) is obtained as follows.

$$\mathbf{J}(x) = \begin{cases} D\left(\mathbf{H}(x), \mathbf{A}, t(x)\right), & \Delta(\mathbf{A}) \le \Delta(\mathbf{A}_{WB}) \\ W\left[D\left(\mathbf{H}(x), \mathbf{A}_{WB}, t(x)\right)\right], & \text{otherwise} \end{cases}. \quad (22)$$

Fig. 6 shows examples of the proposed dehazing method. Fig. 6(a) presents an example of dehazing method for hazy image with no chromatic veil. The Δ value of **A** is smaller than that of $\mathbf{A}_{WB}$, that is, $\Delta(A) \le \Delta(A_{WB})$. In this case, haze removal is performed by the dehazing function $D(\mathbf{H}(x),\mathbf{A},t(x))$. From Fig. 6(a), the dehazing method of $\mathbf{J}=D(\mathbf{H}(x),\mathbf{A},t(x))$ is a good choice (red box) when $\Delta(\mathbf{A}) \le \Delta(\mathbf{A}_{WB})$. In Fig. 6(b), the difference in **A** is $\Delta(\mathbf{A})=0.411$, whereas $\Delta(\mathbf{A}_{WB})=0.045$. From this result, it is expected that a color veil contaminates the image. From Fig. 6(b), the dehazing method of $W[D(\mathbf{H}(x),\mathbf{A}_{WB},t(x))]$ (red box) is better than the common dehazing function. In summary, Δ of

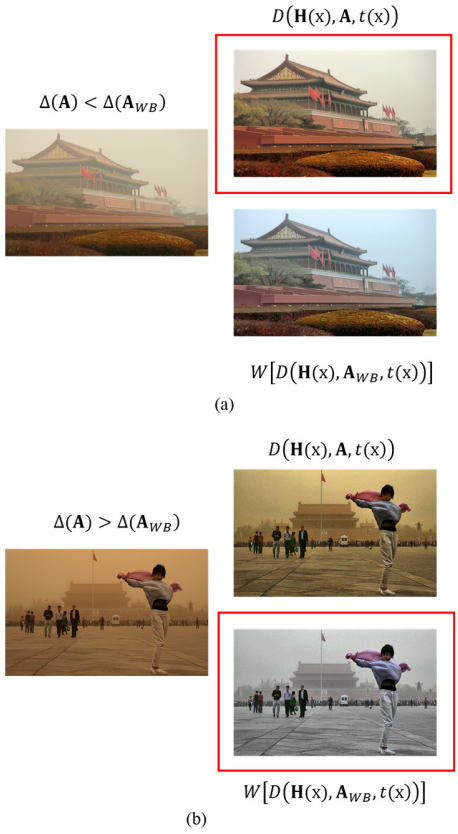

Fig. 6. Examples of colored veil removing approach. (a) dehazing method for a hazy image with no chromatic veil, and (b) dehazing method for a hazy image with chromatic veil.

the atmospheric light plays an important role in achieving good dehazing performance. The proposed method can remove haze adaptively depending on the type of atmospheric veil.

E. Effect of Atmospheric Light

Fig. 7 shows two dehazed image using the DCP algorithm with different **A** (He *et al.*'s **A** [19] and Tang *et al.*'s **A** [32]). The DCP-based dehazing results have annoying artifacts in the sky as shown in Fig. 7(a). On the other hand, the same dehazing function with different **A** (Tang *et al.*'s **A**) alleviates the annoying artifact as shown in Fig. 7(b). This is due to the median filtering for all the 0.1% pixels with the largest dark channel values. In conclusion, the DCP method shows different dehazing results depending on **A**.

In this paper, we calculate the intensity and saturation using the image normalized by **A**, and estimate $t(x)$ based on these two components as shown in (14). In addition, we assume that atmospheric light **A** is given. An estimation of atmospheric light does not affect the proposed method very much. Fig. 8 shows an example. The atmospheric light is estimated using three methods (Tang *et al.*'s [32], quad-tree subdivision-based [47], and He *et al.*'s method [19]). As shown in Fig. 8, the dehazing results are similar. These results show that the proposed method is relatively unaffected by the estimation of

This article has been accepted for publication in a future issue of this journal, but has not been fully edited. Content may change prior to final publication. Citation information: DOI 10.1109/TIP.2019.2948279, IEEE Transactions on Image Processing

(a) (b) (c)

Fig. 7. Dehazing result based on the DCP method using different **A**. (a) hazy image, (b) dehazed image using He *et al*.'s **A** [19], and (c) dehazed image using Tang *et al*.'s **A** [32].

(a) (b) (c) (d)

Fig. 8. Dehazing result based on the proposed method using different **A**. (a) hazy image, (b) dehazed image using Tang *et al*.'s **A** [32], (c) dehazed image using quad-tree subdivision-based **A** [47], and (d) dehazed image using He *et al*.'s **A** [19].

A.

F. Summary of Proposed Method

Table I lists the overall algorithm of the proposed dehazing method. The atmospheric light is estimated from the observed hazy image. The method reported by by Tang *et al*. [32] is used to estimate the atmospheric light. A white balanced hazy image is obtained using the gray-world assumption shown in (21), and the atmospheric light for the white balanced image is estimated. The deviations of the two obtained atmospheric lights are compared, and one of the two methods of haze removal is selected automatically, as shown in Step 5) in Table I. The dehazing results of the proposed method are obtained using (22). Finally, contrast limited adaptive histogram equalization (CLAHE) can be applied to enhance the brightness component.

TABLE I
OVERALL ALGORITHM OF THE PROPOSED METHOD

Input: hazy image **H**
Output: dehazed image **J**
1) Obtain **A** from **H**.
2) Obtain white balanced hazy image $\mathbf{H}_{WB}$ using (21).
3) Obtain $\mathbf{A}_{WB}$ from $\mathbf{H}_{WB}$.
4) Compute $\Delta(\mathbf{A})$ and $\Delta(\mathbf{A}_{WB})$
5) If $\Delta(\mathbf{A}) < \Delta(\mathbf{A}_{WB})$
   A. Obtain normalized hazy image $\mathbf{H}_n$ with **A**.
   B. Estimate saturation of $\mathbf{H}_n$ using (18), (19), or (20).
   C. Compute transmission map using (14).
   D. Obtain dehazed image using $\mathbf{J}=D(\mathbf{H}(x), \mathbf{A}, t(x))$.
   Else
   A. Obtain normalized hazy image $\mathbf{H}_n$ with $\mathbf{A}_{WB}$.
   B. Estimate saturation of $\mathbf{H}_n$ using (18), (19), or (20).
   C. Compute transmission map using (14).
   D. Obtain dehazed image $\mathbf{J}=W[D(\mathbf{H}(x), \mathbf{A}_{WB}, t(x))]$.
6) Apply CLAHE (optional).

IV. SIMULATION RESULTS

To verify the effectiveness of the proposed dehazing approach, is was tested on various types of hazy images. Test images were composed of natural hazy images, synthetic hazy images, natural images with color veils, outdoor dehazing benchmark dataset (O-HAZE) [48], and a large-scale benchmark for realistic single image dehazing (RESIDE) [49]. The performance of the proposed method is compared with that of various state-of-the-art dehazing methods, namely, the efficient multi-scale correlated wavelet approach (MSCW) [13], DCP [19], boundary constrained context regularization (BCCR) [29], HL [33], NLD [34], CAP [44], fast visibility restoration (FVR) [50], artificial multiple-exposure image fusion (AMIF) [51], night-time dehazing by fusion (NDF) [52], and gradient residual minimization (GRM) [53]. Furthermore, the performance of our algorithm is also compared with that of machine learning-based dehazing approaches, namely, DehazeNet [35], MSCNN [36], AOD-Net [37], DCPDN [38], GFN [39], FPCNN [40], strong baseline for single image dehazing (SBID) [41], DDN [42], PDN [43], and enhanced pix2pix dehazing network (EPDN) [54].

A. Computation Time

The proposed method was implemented on Intel i5-7500 CPU @ 3.40GHz and 8G RAM without a CPU or multithreading acceleration. The code was written in un-optimized Python in the Window 10 environment. The existing methods to be compared were implemented in the same environment. All codes are available on the Internet. The execution time was averaged per ten execution times, and the times for reading and writing images were excluded. Only the test time for the machine learning-based dehazing approaches were measured. The DCP [19] was implemented using a guided filter instead of soft matting for the transmission map refinement. Table II presents the execution times for various image sizes. As shown in Table II, the proposed approach is significantly faster than the other algorithms. Even when the given hazy image is large, the proposed method achieves a faster processing time.

B. Qualitative Comparison on Natural Images

The end-to-end dehazing results on challenging natural images are presented. Figs. 9 shows a qualitative comparison of our results with those of fifteen state-of-the-art dehazing methods. DCP [19] does not generate good dehazing performance. This method has a poor performance, especially in the background region, such as sky. BCCR [29] results in a significant amount of color shift in the restored images. FVR [50] effectively removes most of the haze, and restores the details of the scenes and objects. However, the dehazing results

This article has been accepted for publication in a future issue of this journal, but has not been fully edited. Content may change prior to final publication. Citation information: DOI 10.1109/TIP.2019.2948279, IEEE Transactions on Image Processing

TABLE II
EXECUTION TIMES OF VARIOUS ALGORITHMS (UNIT: SECOND)

	Image size					
Method	408x512	786x1024	1193x1590	1536x2048	2304x3072	2034x4032
MSCW [13]	0.213	0.810	2.150	3.659	8.219	14.589
DCP [19]	3.626	12.878	33.780	56.851	129.418	222.965
BCCR [29]	1.527	5.661	15.304	25.725	57.222	89.719
NLD [34]	5.472	11.198	19.836	29.113	57.727	239.123
CAP [41]	0.614	2.209	5.555	9.479	21.321	36.167
FVR [50]	3.362	44.967	236.482	804.323	3540.866	8028.500
AMIF [51]	1.527	5.661	15.304	25.725	57.222	89.719
DehazeNet [35]	1.842	6.743	17.622	29.392	76.612	145.754
MSCNN [36]	1.482	5.297	21.379	28.556	362.530	1019.745
Proposed	**0.071**	**0.345**	**0.866**	**1.594**	**3.642**	**5.950**

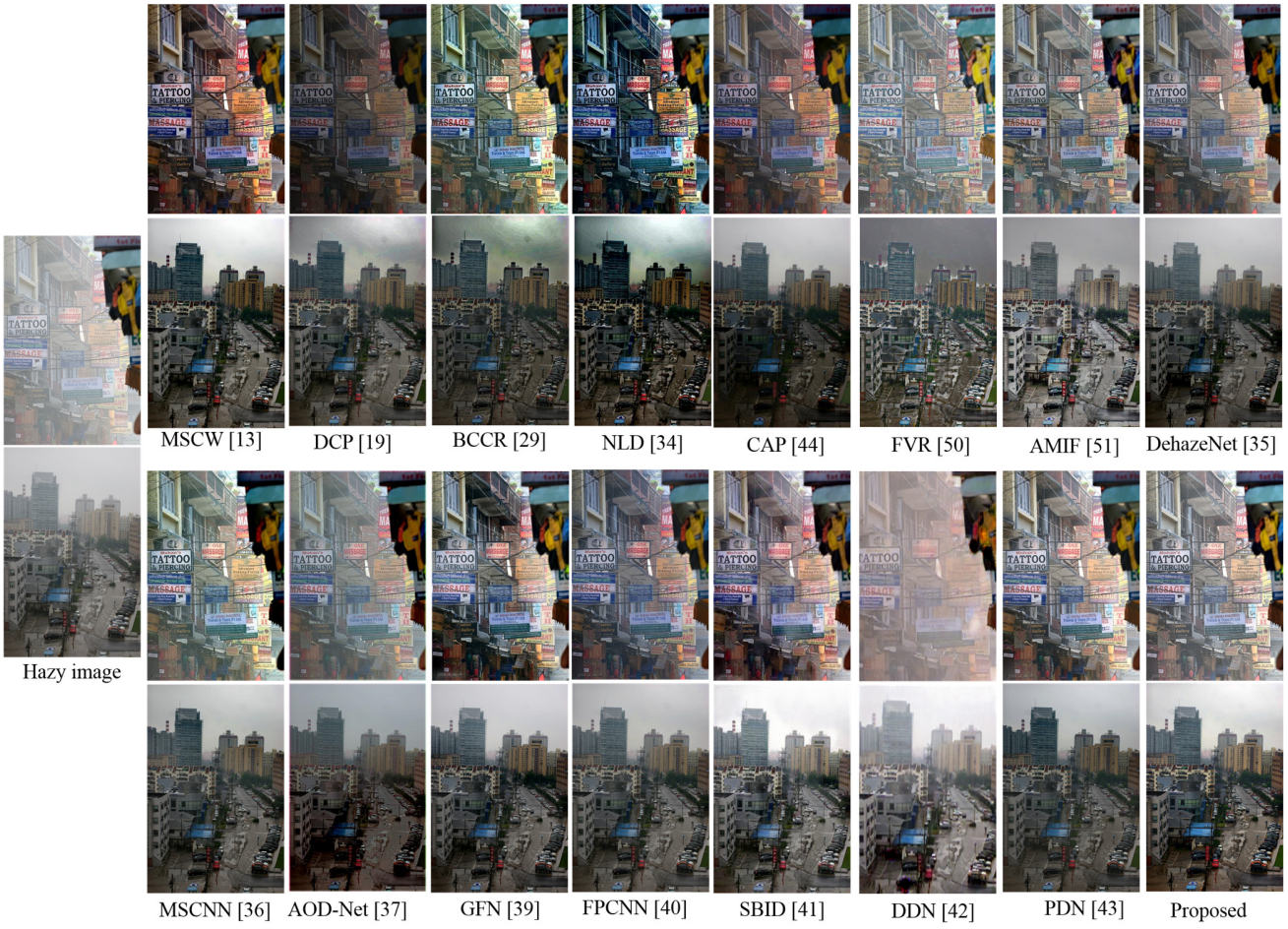

Fig. 9. Performance comparison of various single image dehazing methods using sample natural images.

suffer from over-enhancement, which generates halo artifacts near discontinuities. The three dehazing algorithms mentioned above are based on DCP. Owing to the limit of assumption of DCP, these three methods show relatively low haze removal performance.

CAP [44] presents a rapid dehazing algorithm based on a color attenuation prior. This method does not remove haze in images sufficiently and causes a color shift as shown in Fig. 9. MSCW [13] removes the haze quite well, and restores the image details properly. AMIF [51] uses an artificial multiple-exposure image fusion for image dehazing. This algorithm is fast and shows good dehazing performance. However, this method does not restore the details of the image fully. NLD [34] restores image the detail quite well, but, this method tends to overestimate the detail of the image and has a weak point in restoring the uniform region.

As shown in Fig. 9, machine learning-based dehazing approaches do not show annoying artifacts except for SBID

This article has been accepted for publication in a future issue of this journal, but has not been fully edited. Content may change prior to final publication. Citation information: DOI 10.1109/TIP.2019.2948279, IEEE Transactions on Image Processing

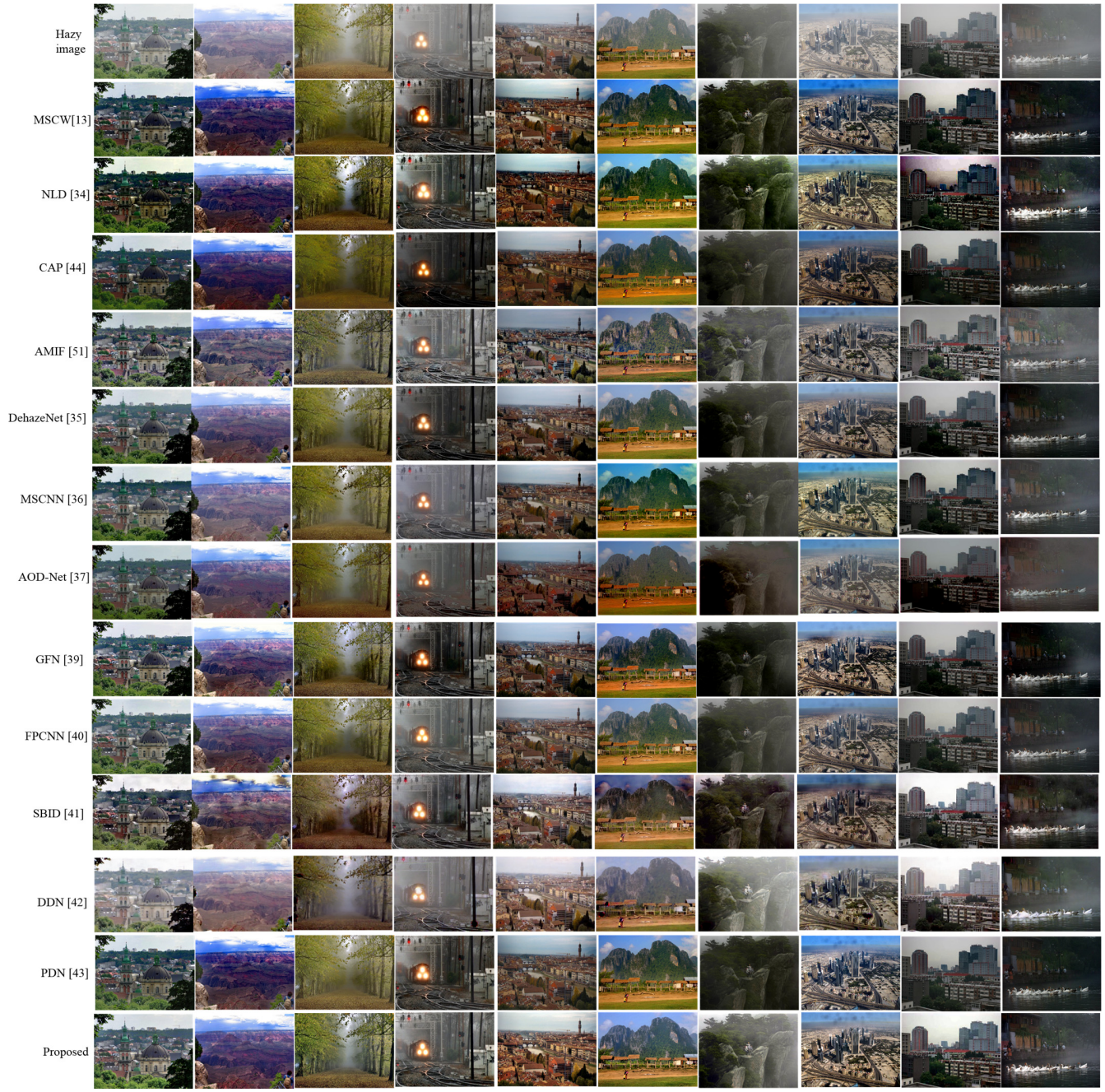

Fig. 10. Performance comparison of various single image dehazing methods using sample natural images.

[41]. SBDI has a poor visual result in the background region for some images. DehazeNet [35], MSCNN [36], AOD-Net [37], and DDN [42] cannot fully remove the haze. On the other hand, recently reported machine learning-based dehazing schemes, such as GFN [39], FPCNN [40], and PDN [43], have good dehazing performance. The proposed algorithm has competitive results with these three methods.

For a broader performance comparison, this paper presents the haze removal results for ten popular natural images in Fig 10. From Fig 10, the dehazing results using the proposed algorithm are competitive or superior to those of other methods in terms of the haze removal capability, detail recovery, color shift, and uniform region recovery. The advantages of the proposed method are significant when considering the computation time.

C. *Qualitative Comparison on Synthetic Images*

Fig. 11 presents the image dehazing results for various synthetic images. MSCW [13], and NLD [34] recover the image details well. However, these two methods cannot remove the color veils shown in the fourth, and fifth columns of Fig. 12. GFN [39] and SBID [41] recover image details well, but they have visually uncomfortable artifacts. FPCNN [40] and DDN [42] do not fully remove the haze. PDN [43] is good at

This article has been accepted for publication in a future issue of this journal, but has not been fully edited. Content may change prior to final publication. Citation information: DOI 10.1109/TIP.2019.2948279, IEEE Transactions on Image Processing

Fig. 11. Performance comparison of various single image dehazing methods using synthetic images.

Fig. 12. Performance comparison of various single image dehazing methods using natural images with chromatic veil.

removing haze, but fails to remove the color veils. In comparison, the proposed method effectively recovers the image details and removes color veils.

D. Qualitative Comparison on Natural Images with Color Veil

In general, the hazy image is composed of an original image and a light gray veil. In this situation, the atmospheric lights corresponding to each color are similar. However, color veils exist in yellow dust or certain lighting conditions. Almost none of the dehazing approaches consider this situation. Fig. 12 shows dehazing results for natural images with color veils. As shown in Fig. 12, the proposed approach effectively removes the color veils. All methods, except for the proposed method, are unable to remove the color veil.

E. Quantitative Comparison

Ancuti *et al*. [48] generated a dehazing benchmark dataset to evaluate the dehazing performance. In this paper, an outdoor dataset (O-HAZE) composed of 45 images is exploited to quantify dehazing performance. Three evaluation measures are tested, including the peak signal-to-noise ratio (PSNR), structural similarity index (SSIM) [55], and CIEDE2000 color difference [56]. The SSIM evaluates the ability to preserve the structural information of the algorithms, and the CIEDE2000 evaluates the color fidelity. The SSIM ranges from -1 to 1, with a maximum value of one for two identical images. The CIEDE2000 accurately measures the color difference between two images and generates values in the range from zero to 100, with smaller values indicating the better color preservation.

This article has been accepted for publication in a future issue of this journal, but has not been fully edited. Content may change prior to final publication. Citation information: DOI 10.1109/TIP.2019.2948279, IEEE Transactions on Image Processing

TABLE III
QUANTITATIVE COMPARISONS OF VARIOUS ALGORITHMS USING O-HAZE [48] IMAGE DATASET

Method	PSNR (dB)	SSIM	CIEDE2000
DCP [19]	16.586	0.735	20.745
BCCR [29]	17.443	0.753	16.968
HL [33]	-	0.781	16.579
NLD [34]	16.610	0.750	17.088
NDF [52]	16.855	0.747	16.431
DehazeNet [35]	16.207	0.666	17.348
MSCNN [36]	19.068	0.765	14.670
Proposed: $\tau(z,p)$	17.604	0.794	14.169
Proposed: $q(z)$	17.721	0.796	14.039
Proposed: $\eta(z,\gamma)$	17.673	0.794	14.024

Table III presents the average performance of various dehazing algorithms in terms of the PSNR, SSIM, and CIEDE2000. The PSNR, SSIM, and CIEDE2000 values were taken from [34] and [48]. The top three performances are highlighted in red, cyan and blue, respectively. Three dehazing results are obtained using $\tau(z,p)$, $q(z)$, and $\eta(z,\gamma)$. As shown in Table III, the performance of the proposed methods is similar. Our results have the best SSIM and CIEDE2000 values, and have the second highest PSNR performance.

In 2019, Li *et al*. provided the RESIDE benchmark dataset [49]. The RESIDE training set contains 110,500 synthetic hazy indoor images and 313,950 synthetic hazy outdoor images. The RESIDE testing set is composed of a synthetic objective testing set (SOTS) and the hybrid subjective testing set (HSTS), designed to manifest a diversity of evaluation viewpoints. A SOTS includes both the indoor and outdoor images (500 of each). HSTS selects 10 synthetic outdoor hazy images.

The dehazing performance of the SOTS is first compared using PSNR and SSIM. Table IV shows the scores of each algorithm in terms of two full-reference metrics. As shown in Table IV, machine learning-based dehazing approaches generally outperform the image prior-based methods for the SOTS indoor dataset. The SBID [41] has the best PSNR and SSIM scores, and EPDN [54] is following it. The PSNR score of the proposed method is eighth out of sixteen algorithms. On the other hand, the SSIM score of the proposed algorithm ranks fifth, which is three levels higher than our PSNR ranking. For the SOTS outdoor dataset, the proposed dehazing algorithm achieves the best PSNR and SSIM scores. The machine learning-based results of the SOTS outdoor dataset are quite different from those of the indoor dataset. We compared our method with the image prior-based methods in Table V for the HSTS dataset. As shown in Table V, the proposed approach surpasses the second-best methods by a large margin. In addition, the results of the proposed method for the HSTS dataset are similar to those of the SOTS outdoor dataset.

For a subjective evaluation of the RESIDE dataset, the sample images are selected from the HSTS dataset. Fig. 13 shows a qualitative example of dehazed results on a synthetic hazy image. Compared to the clean images, the proposed algorithm generates the closest results to the clean images. Fig. 14 represents a qualitative comparison on a real-world hazy image from HSTS. Even in this case, the proposed dehazing algorithm achieves good haze removal results.

TABLE IV
QUANTITATIVE COMPARISONS OF VARIOUS ALGORITHMS USING RESIDE SOTS [49] IMAGE DATASET

Method	Indoor		Outdoor	
	PSNR (dB)	SSIM	PSNR (dB)	SSIM
DCP [19]	16.62	0.8179		
BCCR [29]	15.72	0.7913		
NLD [34]	17.29	0.7489		
CAP [44]	19.05	0.8364		
FVR [50]	15.72	0.7483		
GRM [52]	18.86	0.8553		
DehazeNet [35]	21.14	0.8472	22.46	0.8514
MSCNN [36]	17.57	0.8102		
AOD-Net [37]	19.06	0.8504	20.29	0.8765
DCPDN [38]	19.13	0.8191	22.49	0.8565
GFN [39]	22.30	0.8800	21.55	0.8444
FPCNN [40]	20.92	0.8729	22.75	0.9014
SBID [41]	27.79	0.9556		
DDN [42]	19.38	0.8242		
EPDN [54]	25.06	0.9232	22.57	0.8630
Proposed	19.93	0.8633	24.96	0.9421

TABLE V
QUANTITATIVE COMPARISONS OF VARIOUS ALGORITHMS USING RESIDE HSTS [49] IMAGE DATASET

Method	PSNR (dB)	SSIM
DCP [19]	14.84	0.7609
BCCR [29]	15.08	0.7382
NLD [34]	18.92	0.7411
CAP [44]	21.53	0.8726
FVR [50]	14.48	0.7642
GRM [52]	18.54	0.7624
Proposed	25.35	0.9429

V. CONCLUSION

In this paper, we proposed a fast and efficient single image dehazing method using saturation-based transmission map estimation. The proposed method does not assume that transmission is constant in a small patch. Therefore, pixel-based medium transmission can be obtained. The normalized atmospheric scattering model with atmospheric light was used, and the minimum operation was applied for the normalized atmospheric scattering model. From this, the transmission map was derived as a function only of the saturation component of the scene radiance. The saturation of scene radiance was estimated using a simple stretching method. Using a simple test, the dehazing performance does not depend largely on the type stretch function. In addition, a color veil removing algorithm using the white balance technique was presented. This method was useful in recovering various hazy images with color veils.

We evaluated various types of hazy images, including natural images, synthetic images, and natural images with color veils. In addition, the performance of the proposed method was compared with that of the existing dehazing algorithms. The simulation results showed that the proposed dehazing scheme outperforms state-of-the-art dehazing approaches in terms of both the computational complexity and dehazing efficiency. Because our algorithm requires no training, prior, and refinement process, we achieved an efficient dehazing algorithm.

This article has been accepted for publication in a future issue of this journal, but has not been fully edited. Content may change prior to final publication. Citation information: DOI 10.1109/TIP.2019.2948279, IEEE Transactions on Image Processing

Fig. 13. Example of dehazed images on a synthetic hazy image from HSTS.

REFERENCES

[1] Y. Y. Schechner, S. G. Narasimhan, and S. K. Nayar, "Instant dehazing of images using polarization," in *Proc. IEEE Conf. Comput. Vis. Pattern Recognit.,* Kauai, Hawaii, USA, 2001, pp. 325-332.

[2] Y. Y. Schechner, S. G. Narasimhan, and S. K. Nayar, "Polarization-based vision through haze," *Appl. Opt*., vol. 42, no. 3, pp. 511–525, 2003.

[3] S. Fang, X. Xia, X. Huo, and C. W. Chen, "Image dehazing using polarization effects of objects and airlight," *Opt. Express*., vol. 22, no. 16, pp. 19523-19537, 2014.

[4] S. G. Narasimhan, and S. K. Nayar, "Chromatic framework for vision in bad weather," in *Proc. IEEE Conf. Comput. Vis. Pattern Recognit.*, Hilton Head Island, SC, USA, 2000, pp. 598–605.

[5] S. G. Narasimhan, and S. K. Nayar, "Contrast restoration of weather degraded images," *IEEE Trans. Pattern Anal. Mach. Intell*., vol. 25, no. 6, pp. 713–724, 2003.

[6] A. M. Reza, "Realization of the contrast limited adaptive histogram equalization (CLAHE) for real-time image enhancement," *VLSI Signal Process*., vol. 38, no. 1, pp. 35–44, 2004.

[7] L. J. Wang, and R. Zhu, "Image defogging algorithm of single color image based on wavelet transform and histogram equalization," *Appl. Math. Sci*., vol. 7, no. 79, pp. 3913-3921, 2013.

[8] A. B. Petro, C. Sbert, and J. M. Morel, "Multiscale Retinex," *IPOL Journal: Image Processing On Line*, pp. 71-88, 2014, 10.5201/ipol.2014.107.

[9] W. T. Yang, R. G. Wang, S. Fang, and X. Zhang, "Variable filter retinex algorithm for foggy image enhancement," *J. Computer-Aided Des. Comput. Graph*, vol. 22, no. 6, pp. 965-971, 2010.

[10] X. Y. Hu, X. H. Gao, and H. B. Wang, "A novel retinex algorithm and its application to fog-degraded image enhancement," *Sens. Transd*., vol 175, no. 7, pp. 138-143, 2014.

[11] Y. Du, B. Guindon, and J. Cihlar, "Haze detection and removal in high resolution satellite image with wavelet analysis," *IEEE Trans. Geosci. Remote Sens*., vol. 40, no. 1, pp. 210-217, 2002.

This article has been accepted for publication in a future issue of this journal, but has not been fully edited. Content may change prior to final publication. Citation information: DOI 10.1109/TIP.2019.2948279, IEEE Transactions on Image Processing

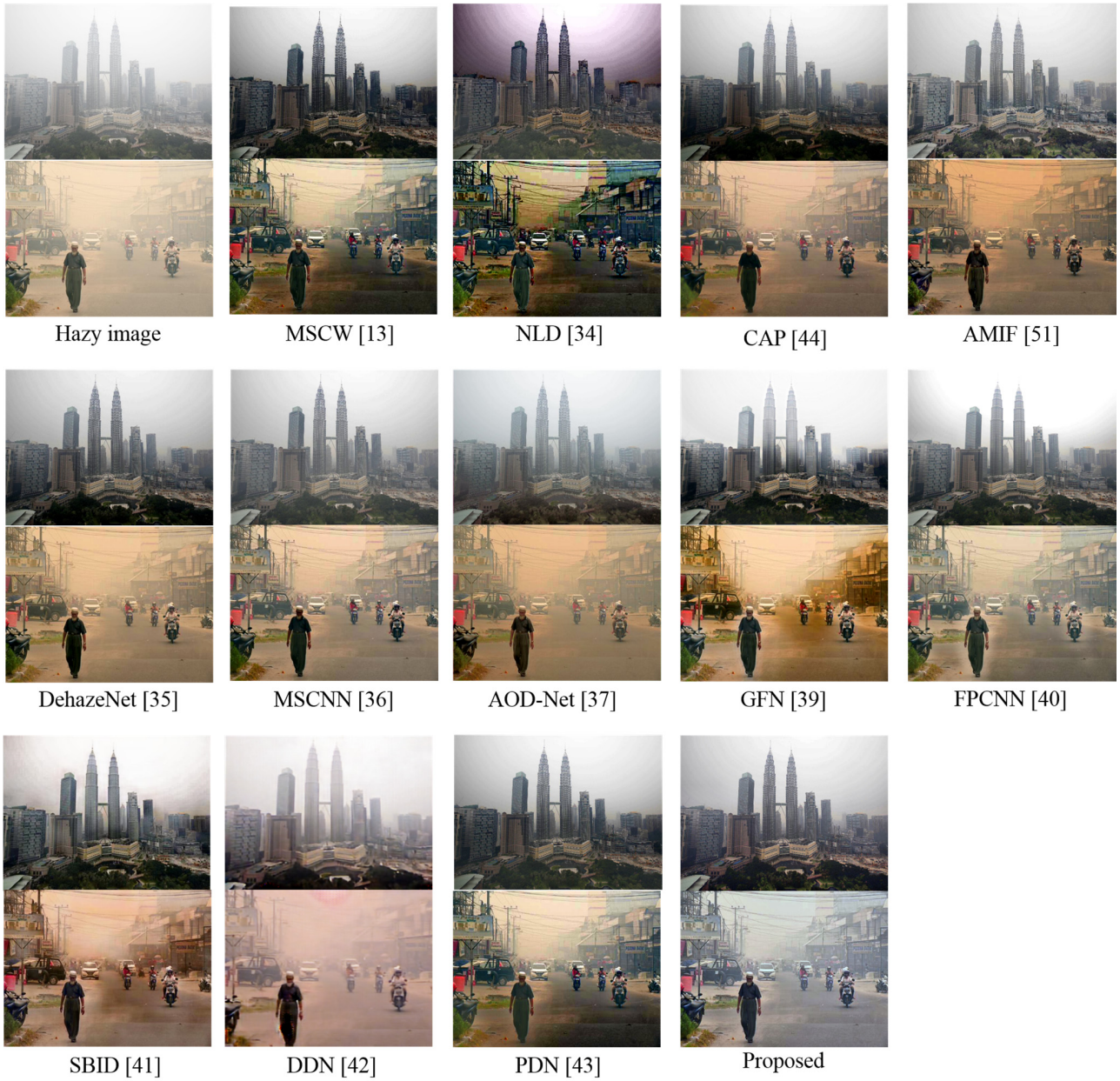

Fig. 14. Example of dehazed images on a real-world hazy image from HSTS.

[12] R. Zhu, and L. J. Wang, "Improved wavelet transform algorithm for single image dehazing," *Optik-Int. J. Light Electron Opt*., vol. 125, no. 13, pp. 3064-3066, 2014.

[13] X. Liu, H. Zhang, Y. M. Cheung, X.You, and Y. Y. Tang, "Efficient single image dehazing and denoising: An efficient multi-scale correlated wavelet approach," *Comput. Vis. Image Underst*., vol. 162, pp. 23-33, 2017.

[14] R. T. Tan, "Visibility in bad weather from a single image," in *Proc. IEEE Conf. Comput. Vis. Pattern Recognit.*, Anchorage, AK, USA, 2008, pp. 1–8.

[15] C. Ancuti and C. O. Ancuti, "Effective contrast-based dehazing for robust image matching," *IEEE Geosci. Remote Sens. Lett.*, vol. 11, no. 11, pp. 1871-1875, 2014.

[16] A. Galdran, J. Vazquez-Corral, D. Pardo, and M. Bertalmio, "A variational framework for single image dehazing," in *Proc. Springer European Conf. Computer Vision*, Zurich, Switzerland, 2014, pp. 259-270.

[17] A. Galdran, J. Vazquez-Corral, D. Pardo, and M. Bertalmio, "Enhanced variational image dehazing," *SIAM J. Imaging Sci.*, vol. 8, no. 3, pp. 519-154, 2015.

[18] R. Fattal, "Dehazing using color-lines," *ACM Trans. Graph.*, vol. 34, no. 3, 2014, Art. no. 13.

[19] K. M. He, J. Sun, and X. O. Tang, "Single image haze removal using dark channel prior," *IEEE Trans. Pattern Anal. Mach. Intell.*, vol. 33, no. 12, pp. 2341-2353, 2011.

[20] C. Xiao, and J. Gan, "Fast image dehazing using guided joint bilateral filter," *Vis.Comput*., vol. 28, no. 6-8, pp. 713–721, 2012.

[21] C. H. Yeh, L. W. Kang, M. S. Lee, and C. Y. Lin, "Haze effect removal from image via haze density estimation in optical model," *Opt. Express*, vol. 21, no. 22, pp. 27127-27141, 2013.

[22] Z. Lin, and X. Wang, "Dehazing for image and video using guided filter," *Appl. Sci*. vol. 2, no. 4B, pp. 123–127, 2012.

[23] R. J. Gao, X. Fan, J. L. Zhang, and Z. X. Luo, "Haze filtering with aerial perspective," in *Proc. IEEE Int. Conf. Image Process.*, Orlando, FL, USA, 2012, pp. 989-992.

[24] S. C. Huang, B. H. Chen, and W. J. Wang, "Visibility restoration of single hazy images captured in real-world weather conditions," *IEEE Trans. Circuits Syst. Video Technol.*, vol. 24, no. 10, pp. 1814-1824, 2014.

[25] J. B. Wang, N. He, L. L. Zhang, and K. Lu, "Single image dehazing with a physical model and dark channel prior," *Neurocomputing*, vol. 149, pp.

718-728, 2015.

[26] H. Zhang, X. Liu, Z. T. Huang, and Y. F. Ji, "Single image dehazing based on fast wavelet transform with weighted image fusion," in *Proc. IEEE Int. Conf. Image Process.*, Paris, France, 2014, pp. 4542-4546.

[27] H. B. Liu, J. Yang, Z. P. Wu, and Q. N. Zhang, "Fast single image dehazing based on image fusion," *J. Electron. Imaging*, vol. 24, Article ID 013020, 2015.

[28] K. B. Gibson, D. T. Vo, and T. Q. Nguyen, "An investigation of dehazing effects on image and video coding," *IEEE Trans. Image Proc.*, vol. 21, no. 2, pp. 662-673, 2012.

[29] G. F. Meng, Y. Wang, J. Y. Duan, S. M. Xiang, and C. H. Pan, "Efficient image dehazing with boundary constraint and contextual regularization," in *Proc. IEEE Int. Conf. Comput. Vis.*, Sydney, NSW, Australia, 2013, pp. 617-624.

[30] S. M. Lee, S. M. Yun, J. H. Nam. C. S. Won, and S. W. Jung, "A review on dark channel prior based image dehazing algorithms," *EURASIP J. Image Video Process*., vol. 2016:4, pp. 1-23, 2016.

[31] Y. Bahat and M. Irani, "Blind dehazing using internal patch recurrence," in *Proc. IEEE ICCP*, Evanston, IL, USA, 2016, pp. 1-9.

[32] K. Tang, J. Yang, and J.Wang, "Investigating haze-relevant features in a learning framework for image dehazing," in *Proc. IEEE Conf. Comput. Vis. Pattern Recognit.,* Columbus, OH, USA, 2014, pp. 2995-3002.

[33] D. Berman, T. Treibitz, and S. Avidan, "Single image dehazing using haze-lines," *IEEE Trans. Pattern Anal. Mach. Intell.*, to be published. DOI: 10.1109/TPAMI.2018.2882478.

[34] D. Berman, T. Treibitz, and S. Avidan, "Non-local image dehazing," in *Proc. IEEE Conf. Comput. Vis. Pattern Recognit.,* Las Vegas, NV, USA, 2016, pp. 1674-1682.

[35] B. Cai, X. Xu, K. Jia, C. Qing, and D. Tao, "DehazeNet: An end-to-end system for single image haze removal," *IEEE Trans. Image Process.*, vol. 25, no. 11, pp. 5187–5198, 2016.

[36] W. Ren, S. Liu, H. Zhang, J. Pan, X. Cao, and M.-H. Yang, "Single image dehazing via multi-scale convolutional neural networks," in *Proc. Eur. Conf. Comput. Vis.*, 2016, pp. 154–169.

[37] B. Li, X. Peng, Z. Wang, J. Xu, and D. Feng, "AOD-Net: All-in-one dehazing network," in *Proc. IEEE Int. Conf. Comput. Vis.*, Venice, Italy, 2017, pp. 4780–4788.

[38] H. Zhang and V. M. Patel, "Densely connected pyramid dehazing network," " in *Proc. IEEE Conf. Comput. Vis. Pattern Recognit.*, Salt Lake City, UT, USA, 2018, pp. 3253-3261.

[39] W. Ren, L. Ma, J. Zhang, J. Pan, X. Cao, W. Liu, and M.-H. Yang, "Gated fusion network for single image dehazing," in *Proc. IEEE Conf. Comput. Vis. Pattern Recognit.*, Salt Lake City, UT, USA, 2018, pp. 3194-3203.

[40] J. Zhang, Y. Cao, Y. Wang, C. Wen, and C. W. Chen., "Fully pointwise convolutional neural network for modeling statistical regularities in natural images," in *Proc. ACM Conf. Multimedia*, Seoul, Korea, 2018, pp. 984-992.

[41] Z, Xu, X. Yang, X. Li, X, Sun, and P. R. Harbin, "Strong baseline for single image dehazing with deep features and instance normalization," in *Proc. British Machine Vision, Conference*, Newcastle, UK, 2018.

[42] X. Yang, Z. Xu, and J. Luo, "Towards perceptual image dehazing by physics-based disentanglement and adversarial training," in *Proc. Thirty-Second AAAI Conference on Artificial Intelligence*, New Orleans, LA, USA, 2018, pp.7485-7492.

[43] D. Yang, and J. Sun, "Proximal Dehaze-Net: A prior learning-based deep network for single image dehazing," in *Proc. the European Conference on Computer Vision*, Munich, Gernay, 2018, pp. 702-717.

[44] Q. Zhu, J. Mai, and L. Shao, "A fast single image haze removal algorithm using color attenuation prior," *IEEE Trans. Image Process*., vol. 24, no. 11, pp. 3522–3533, 2015.

[45] L. Y. He, J. Z. Zhao, and D. Y. Bi, "Effective haze removal under mixed domain and retract neighborhood," *Neurocomputing*, vol. 293, pp. 29-40, 2018.

[46] S.G. Narasimhan and S.K. Nayar, "Vision and the Atmosphere," *Int'l J. Computer Vision*, vol. 48, pp. 233-254, 2002.

[47] J. H. Kim, W. D. Jang, J. Y. Kim, and C. S. Kim, "Optimized contrast enhancement for real-time image and video dehazing," *J. Vis. Commun. Image R*., vol. 24, no. 3, pp. 410-425, 2013.

[48] C. O. Ancuti, C. Ancuti, R. Timofte, and C. D. Vleeschouwer, "O-HAZE: a dehazing benchmark with real hazy and haze-free outdoor images," in *Proc. IEEE Conf. Comput. Vis. Pattern Recognit.*, Salt Lake City, UT, USA, 2018, pp. 867-875, 2018.

[49] B. Li, W. Ren, D. Fu, D. Tao, D. Feng, W. Zeng, and Z. Wang, "Benchmarking single image dehazing and beyond," *IEEE Trans. Image Process.*, vol. 29, no. 1, pp. 492–505.

[50] J. P. Tarel and N. Hautiere, "Fast visibility restoration from a single color or gray level image," in *Proc. IEEE 12th Int. Conf. Comput. Vis.,* Kyoto, Japan, 2009, pp. 2201–2208.

[51] A. Galdran, "Image dehazing by artificial multiple-exposure image fusion," *Signal Process*., vol. 149, pp. 135–147, 2018.

[52] C. Ancuti, C. O. Ancuti, C. De Vleeschouwer, and A. C. Bovik, "Night-time dehazing by fusion," in *Proc. IEEE Int. Conf. Image Process.*, Phoenix, AZ, USA, 2016, pp. 2256-2260.

[53] C. Chen, M. N. Do, and J. Wang, "Robust image and video dehazing with visual artifact suppression via gradient residual minimization," in *Proc. the European Conference on Computer Vision*, Amsterdam, Netherlands, 2016, pp. 576-591.

[54] Y. Qu, Y. Chen, J. Huang, and Y. Xie, "Enhanced pix2pix dehazing network," in *Proc. IEEE Conf. Comput. Vis. Pattern Recognit.*, Long Beach, CA, USA, 2019, pp. 8160-8169.

[55] Z. Wang, A. C. Bovik, H. R. Sheikh, and E. P. Simoncelli, "Image quality assessment: from error visibility to structural similarity, *IEEE Trans. Image Process.*, vol. 13, no. 4, pp. 600–612, 2004.

[56] G. Sharma, W. Wu, and E. N. Dalal, "The ciede2000 colordifference formula: Implementation notes, supplementary test data, and mathematical observations," *Color Res. Appl*., vol. 30, no. 1, pp. 21–30, 2005.